

NANO EXPRESS

Open Access

Synthesis of colloidal solutions with silicon nanocrystals from porous silicon

José Alberto Luna López*, Abel Garzón Román, Estela Gómez Barojas, JF Flores Gracia, Javier Martínez Juárez and Jesús Carrillo López

Abstract

In this work, we have obtained colloidal solutions of Si nanocrystals (Si-ncs), starting from free-standing porous silicon (PSi) layers. PSi layers were synthesized using a two-electrode Teflon electrochemical cell; the etching solution contained hydrogen peroxide 30%, hydrofluoric acid 40% (HF), and methanol. The anodizing current density was varied to 250 mA cm^{-2} , 1 A cm^{-2} , and 1.2 A cm^{-2} . Thus obtained, PSi was mechanically pulverized in a mortar agate; then, the PSi powders were poured into different solutions to get the final Si-ncs colloidal solutions. The different optical, morphological, and structural characteristics of the colloidal solutions with Si-ncs were measured and studied. These Si-ncs colloidal solutions, measured by photoluminescence (PL), revealed efficient blue-green or violet emission intensities. The results of X-ray diffraction (XRD) indicate that the colloidal solutions are mainly composed of silicon nanocrystallites. The result of UV-vis transmittance indicates that the optical bandgap energies of the colloidal solutions varied from 2.3 to 3.5 eV for colloids prepared in methanol, ethanol, and acetone. The transmission electron microscopy (TEM) images showed the size of the nanocrystals in the colloidal solutions. Fourier transform infrared spectroscopy (FTIR) spectra showed different types of chemical bonds such as Si-O-Si, Si-CH₂, and SiH_x, as well as some kind of defects.

Keywords: Colloidal solution; Silicon nanocrystal; XRD; PL; FTIR

PACS: 61.46Df.-a; 61.43.Gt; 61.05.cp; 78.55.-m; 81.15.Gh

Background

The research of nanoparticles with unique dimensionality dependent on the chemical-physical properties of nanoscale matter has propelled efforts towards controllable fabrication and in-depth characterization of inorganic nanostructures with desirable compositional and geometric features. At the forefront of the current scientific revolution of colloidal nanocrystals (C-nc), crystalline particles grown in liquid media stand out over other classes of inorganic nanomaterials due to the high degree of control with which their crystal structure, size, shape, and surface functionalities can be engineered in the synthesis stage and to the versatility with which they can be processed and implemented into a large number of materials and devices [1-3]. On the other hand, silicon is the semiconductor material predominant in the

microelectronics industry. It has an indirect bandgap of 1.1 eV, which is the main limitation for application in optoelectronics and photonics [2], due to low probability of radiative transitions that make silicon a poor light emitter. However, unlike bulk silicon, silicon nanoparticles (silicon nanocrystals) have a behavior as a direct bandgap semiconductor [4,5]. After the discovery of visible light emission at room temperature in the porous silicon (PSi) by Canham [6] in 1990, many researchers have studied the emission properties of materials with Si nanocrystals (Si-ncs). Among many techniques to prepare Si-ncs, the electrochemical etching of porous Si remains the cheapest and fastest method; it may be the most promising for production of large amounts of Si-ncs required for potential applications in nanotechnology. Silicon-rich oxide (SRO) has shown photoemission. But it required normally a high-temperature annealing in order to get intense emission. Also, Si-ncs obtained by electrochemical methods and poured in solutions have shown photoemission that depends on their size.

* Correspondence: jose.luna@correo.buap.mx

Instituto de Ciencias, Centro de Investigaciones en Dispositivos Semiconductores, Benemérita Universidad Autónoma de Puebla, Ed. 103C o D, Ciudad Universitaria, Col. San Manuel, Puebla, Puebla C.P. 72570, México

Thus, Si-ncs obtained by electrochemical methods are an alternative to obtain emission different to the ones of silicon-rich oxide but without a high-temperature annealing [7]. Colloidal dispersions containing monodispersed and polydispersed nanoscale particles are of great importance in the field of nanoscience and nanotechnology [8,9]. Their main characteristics are the well-defined dimensions and extraordinary functional properties [8,9], which have started to be used to elucidate the properties of colloidal matter [10]. In addition, particles with uniform structural properties are offering best properties for applications in different fields such as catalysis [11,12], gas sensors [13], biosensors [14], magnetic materials [15], and photonics [16] among others [17,18]. Significant efforts in this direction are being made to develop simple and reproducible methods capable of generating colloidal samples monodispersed and polydispersed in small and large quantities [8-10,19] based on colloidal chemistry [17,20]. The method we use for the synthesis of colloidal silicon nanocrystals (C-Si-ncs) is novel in many ways, because unlike other methods, this is easier to implement, fast, cheap, and has good control on the parameters used, unlike other well-known methods such as Stober, laser pulsed, controlled precipitation, emulsions, oxidation, combustion of silane, gas evaporation, and thermal degradation [21-34]. Also, in this work, we prove and present that using different solvents in the solutions results different behaviors, such as the change of color of the samples without the excitation. The photoluminescence (PL) (change in the emission wavelength) of the C-Si-ncs changes with the excitation wavelength, and this is another important optical property. Therefore, the goal of this work is to study and investigate the compositional and optical properties of C-Si-nc suspensions formed with pulverized porous Si layers, when the Si-nc powders are suspended in different organic solvents. Special attention is paid to a surprising observation of intense green and blue PL in C-Si-nc suspensions, which opens the possibility to propose novel applications in a future work.

Methods

PSi powder has been prepared by standard electrochemical etching of Si wafers (<100> p-type, $\rho = 0.01$ to $0.02 \Omega \text{ cm}$ and diameter 2 in). Before the electrochemical etching, the wafers were cleaned in three different solutions (xylene, acetone, and methanol) for 11 min in ultrasonic bath and then the wafers were rinsed with deionized water. The solution to obtain PSi consisted of a mixture of peroxide of hydrogen/hydrofluoric acid (HF)/methanol (2:1:1).

The experimental method was realized as that of Valenta et al. [35]. We used an electrolytic cell of Teflon

with a platinum electrode (cathode) and a brass electrode (anode), which has a current source, and then the solution was poured into the cell and a current in the source terminals is applied to the electrodes (anode and cathode) for the electrochemical reaction. The etching current density was varied to obtain a higher porosity and thickness. The current densities used to obtain the samples were varied from 250 mA cm^{-2} , 1.0 A cm^{-2} , 1.2 A cm^{-2} , and 1.28 A cm^{-2} . We used a short time (between 10 and 15 min) if a high-density current ($>1.0 \text{ A cm}^{-2}$) was used. Once the PSi layer was obtained, we rinsed it with deionized water to stop the chemical process. The samples obtained are listed in Table 1. After, the PSi films so obtained were scraped off the silicon wafer and subsequently milled in an agate mortar. The obtained powders were mixed together with the solvent selected. Then, we wait for around 2 weeks until the larger particles were decanted. This process can be accelerated using a centrifuge equipment. Colloidal solutions were prepared by pouring the powder in three different organic solvents (ethanol, methanol, and acetone). Finally, almost transparent solutions with intense green and blue PL under UV excitation were obtained. Such C-Si-nc suspensions are a starting point for production of various Si nanostructures with colloidal phase.

The PL response was measured at room temperature using a Horiba Jobin Yvon spectrometer model FluoroMax 3 (Edison, NJ, USA) with a pulsed xenon excitation source and a multiplier tube detector controlled by a computer. The samples were excited using a radiation of 250 nm, and the PL response was recorded in the range from 400 to 900 nm with a resolution of 1 nm. Room-temperature transmittance spectra of the colloidal Si-nc suspensions were measured using an Cary 5000 UV-vis-NIR system (Agilent Technologies Inc., Santa Clara, CA, USA). The transmittance spectra were recorded in the range from 350 to 900 nm with a resolution of 0.5 nm. Fourier transform infrared spectroscopy (FTIR) was measured in the range from 450 to $4,000 \text{ cm}^{-1}$ using a Bruker system model Vector 22 (Bruker Instruments, Billerica, MA, USA).

Table 1 Samples of C-Si-nc suspensions to different current densities and different solvents

Sample	Current density (A cm^{-2})	Solvent	Porosity (%)	Thickness (μm)
M-09	1.20	Methanol	70	12
M-10	1.28	Acetone	67	11
M-14	0.25	Ethanol	99	98
M-16	1.00	Acetone	96	41
M-17	1.00	Acetone	92	15
M-19	1.28	Acetone	65	8

The X-ray diffraction (XRD) diffractograms were obtained with a D8 discover Bruker diffractometer operated at 40 kV and at 40 mA using the CuK α 1 radiation (1.5406 Å). The powder with Si-ncs diffractograms were recorded to 2θ , which was varied from 5° to 80° in 0.02° step size (Bruker Instruments). The TEM images were obtained with JEOL-2010 HRTEM (Jeol, Tokyo, Japan), with a potential of 200 kV.

Results and discussion

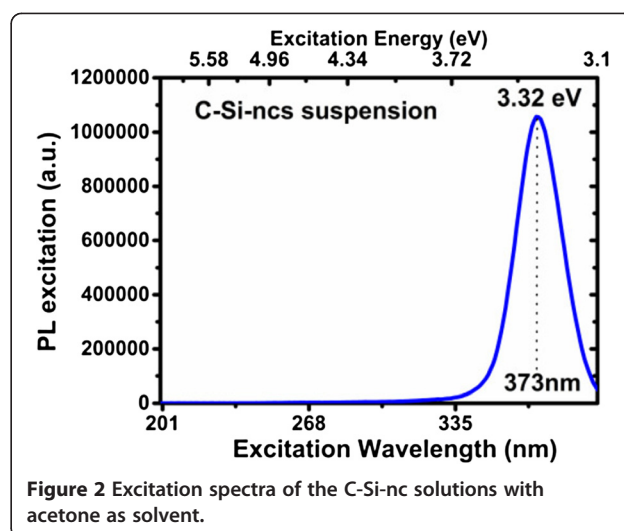
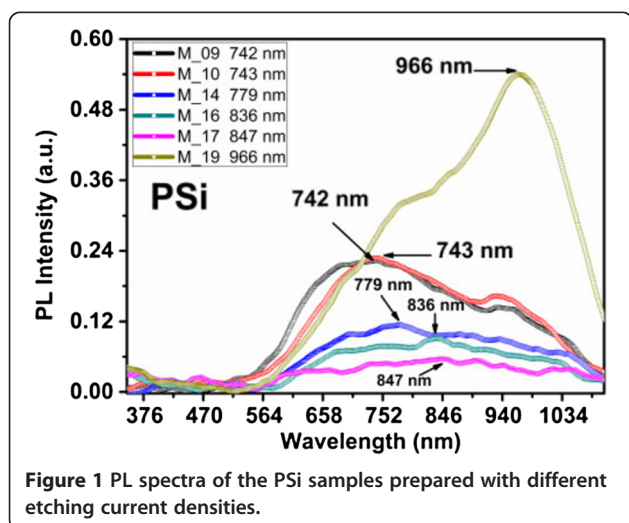
The PSi samples showed intense near-infrared PL spectra under UV excitation; all samples have a Gaussian-like shape with the maximum peak located between 743 and 966 nm, depending on the sample, as shown in Figure 1.

In Table 1, some preparation parameters of the PSi single layers and the C-Si-nc solutions are listed. Also, the results of porosity and thickness obtained by gravimetry [36] are listed. Below, we present the results and their discussion for the results with the different characterization techniques used.

Photoluminescence

The C-Si-nc solutions with different solvents were first excited with different selected wavelengths from 200 to 400 nm to find the appropriate excitation wavelength. Then, the PL spectra were measured. Figure 2 shows an excitation spectrum of the C-Si-nc suspension with acetone as solvent.

The C-Si-nc suspensions with different solvents show intense green, blue, and violet PL intensities, which depend on the solvent used. A similar PL behavior is observed in the infrared range, but in this case, the red PL intensity is smaller than the green-violet PL intensity, as shown in Figure 3a. It is important to note that based on the PL results, the process is repetitive; the similarity between the spectra of samples M-16 and M-19 and



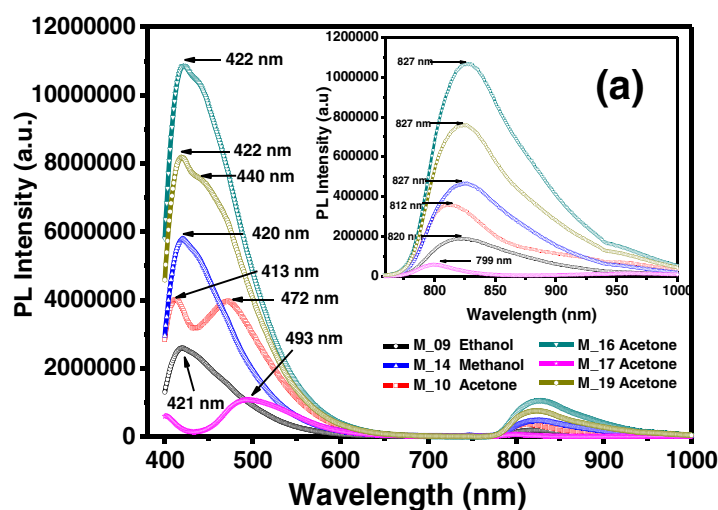
samples M-10 and M-17 confirms this. The colors of the C-Si-nc solutions are shown in Figure 3b. It is seen that M-16 is the most transparent solution and M-17 is the darkest solution. The PL intensity is related with this behavior. We can infer from this figure that the solution with the greatest PL intensity is the sample M-16.

As can be seen in the inset of Figure 3a, the PL spectra have a Gaussian-like shape with the maximum peak position lying in the range from 799 nm to 827 nm. The peak position depends on the anodizing current density used to obtain PSi single layers and on the solvent used to obtain the C-Si-nc suspensions. However, it is not possible to observe a clear tendency of the PL intensity with respect to the current density and the solvent used.

All colloidal solutions under UV light show bright green and violet PL emission. The solution M-09 shows an intense PL blue emission that can be observed by the naked eye, and this sample has methanol as solvent. The PL maximum peak is located at 421 nm, and its spectral width extends from 400 to 542 nm; also, it is observed in the spectrum that a secondary PL peak of low intensity is in the near-infrared range with a maximum at 820 nm as we can see in the inset of Figure 3a.

The PL spectrum of the M-10 solution presents three peaks showing a PL maximum peak between green and violet. One peak is located at 413 nm; this wavelength is associated with the violet color and shows an intensity slightly greater than the peak located at 472 nm (second peak, associated with the blue color). The third peak shows a much lower intensity than the former peaks, which is located at 812 nm in the near-infrared region, see the inset in Figure 3a.

The PL spectrum of M-14 solution shows two peaks. The one with greater intensity is located at 420 nm and has a spectral range from 400 to 540 nm, and the other with much lower intensity is located at 827 nm.



(b)

M_09 M_10 M_14 M_16 M_17 M_19

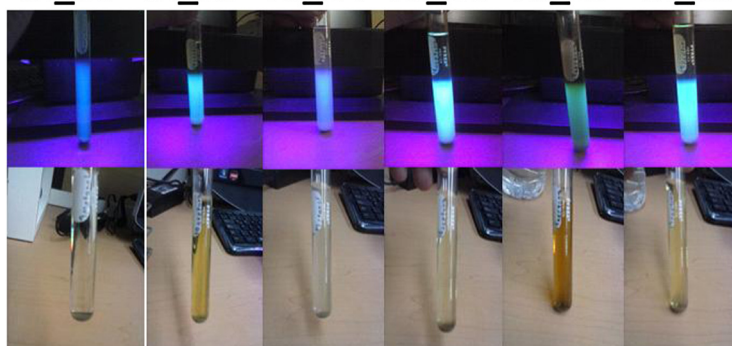


Figure 3 PL spectra of C-Si-nc solutions and their respective colors under room light and UV excitation. (a) PL spectra of C-Si-nc solutions with different solvents. (b) Photographs of the C-Si-nc solutions under room light (lower part) and under UV excitation (upper part).

The spectra of the M-16 and M-19 solutions which were prepared with the acetone as solvent are also shown in Figure 3. The peak with greater intensity is located at 422 nm and corresponds to a spectral range from 400 to 600 nm; and a secondary peak with much lower intensity is located at 827 nm. The PL spectra were obtained with 373-nm excitation radiation. In relation to this result, there are several similar studies that have been reported, such as that of Valenta et al. [35] which has a similar process as in this work, but the results obtained in their PL spectra in orange (like PSi) and PL spectra in green (after being filtered) were wider and with lower intensity due to the particle concentration in the solvent. In our experimental process, the PL intensities appear to be higher. Also, the results of Cortazar Martinez [7] show two peaks: one that is more intense in the blue region and the other in the red region [7], which is less intense. A similar result is reported by Nayfeh et al. [37] and Tilley et al. [38]. These

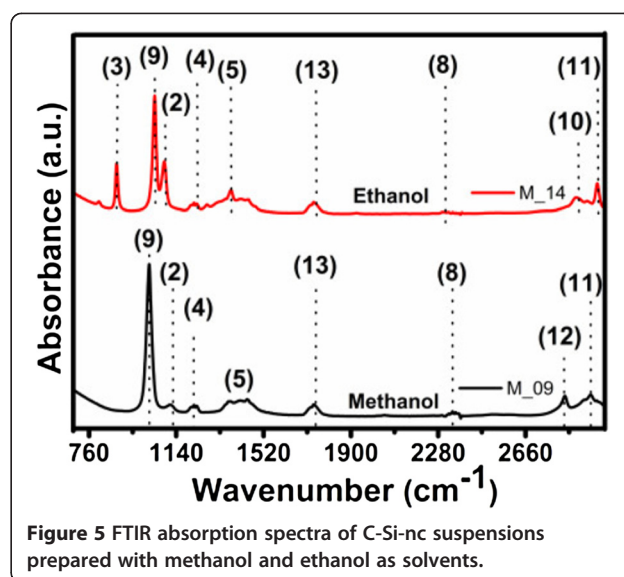
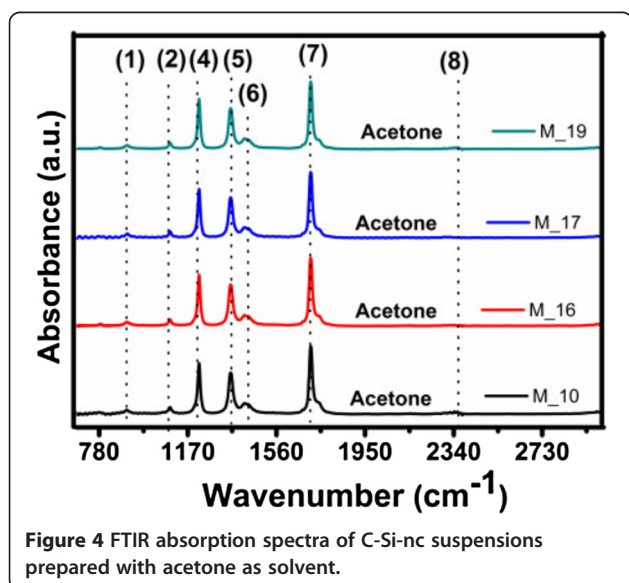
results are due to the mechanical forces applied in an agate mortar to reduce the size of the PSi when it is milled together with the selected solvent. This affects the photoluminescence spectrum of the colloidal solution. Also depending on the applied forces, the Si-nc size differs, where the C-Si-nc suspensions change from transparent to dark, as can be seen in Figure 3b. We obtain changes in the two PL peaks in the violet and near-infrared regions [37,38], where the stronger peak of violet PL dominates due to a larger amount of smaller size nanocrystals and the defects around the nanocrystals. Many models have been proposed to explain the PL such as quantum confinement [4,6,39,40], surface states [41], defects in the oxide [42], and even chemical species [43]. However, the definitive answer to these effects on PL [44] has not been found, but the accepted model is the quantum confinement with exceptions in the nanocrystal size from 1 to 5 nm [40,45]. However, it is difficult to exclude the presence of any thin oxide layer

surrounding the Si-ncs which is necessary to saturate the dangling bonds on the surface or surrounding of the Si-ncs. Therefore, this is generally associated with defect states produced by the process of fabrication. Various authors in the literature have suggested the presence of defects in the samples and assigned an luminescent emission band around 2.7 eV from defect states at the silicon cluster-SiO_x interface; similarly, band emissions around 1.7 eV are also assigned to defects. On the other hand, the hydrogen bonds play an important role in the photoluminescence [46]. In our case, we have a lot of H bonds in the C-Si-nc suspensions structure, as is shown in FTIR spectra.

Fourier transform infrared spectroscopy

The FTIR spectra of the C-Si-nc solutions are shown in Figures 4 and 5. Different Si-O, Si-H, and C-H vibration modes are observed in the spectra of all the samples; but depending on the solvent used, their intensity and peak position change.

The solutions prepared in methanol and ethanol as solvents present additional peaks at around 800 and 1,260 cm⁻¹. These peaks correspond to the vibration frequency of Si-(CH₃)_n bonds. These bonds indicate that the methanol and ethanol molecules are decomposed during the strong milling of the PSi, which generate unbonded Si and CH₃ molecules around the Si-ncs. Therefore, the possible origin of the strong PL intensity of methanol and ethanol suspensions is the Si-ncs related to the Si-(CH₃)_n bonds. On the other hand, C-Si-nc suspensions with acetone show a stronger PL, and their FTIR peaks correspond to vibration frequencies different from those suspensions prepared with methanol as solvent, as shown in Figure 5.



The FTIR absorption spectra of the colloidal solutions are shown in Figure 5. The results of FTIR show different peaks of Si. For example, for the M-09 sample, the PL spectra show peaks at 1,113 cm⁻¹ that correspond to Si-O-Si asymmetric stretching [46-49]. The PL spectra from the M-14 sample show peaks at 880 and 1,088 cm⁻¹ that correspond to O₃SiH bending [47,49] and Si-O-Si asymmetric stretching [46-49], respectively, and for the M-10, M-16, M-17, and M-19 samples, there are peaks found at 900 and 1,092 cm⁻¹ that correspond to SiH₃ degenerate deformation [46-49] and Si-O-Si asymmetric stretching [46-49], respectively. Other peaks appear from organic compounds such as CH₂ asymmetric stretching at 2,800 cm⁻¹ [46] and at about 2,352 cm⁻¹ that correspond to CO₂ bonding [47].

The typical IR active vibrational modes of Si, Si oxide, and Si hydride are listed in Table 2 for comparison and clarity. The assignments of peaks in the FTIR spectra are made on the basis of these signature peaks. Before analyzing the features of interest, we identify the artifacts present in the FTIR spectra and ensure that they do not interfere with the analyses. It is seen that in all the spectra shown in Figures 4 and 5, there are peaks centered at about 2,350 cm⁻¹ which is a typical signature of CO₂ [47]. Serial peaks in the range from 1,390 to 1,800 cm⁻¹ accompanied with a noise-like signal are characteristic of ambient water vapor absorption and Si-CH_n in the samples [47,50]. These signals appear in all spectra due to the adsorption of IR active water vapor and CO₂ molecules from the atmosphere. The intensity and spread (for the water vapor peaks) of these artifact IR active bands vary for the different samples, indicating different amounts of absorption during sample formation. As these peaks do not interfere with the peaks of interest, they are only considered as a reference. The FTIR

Table 2 FTIR spectra of C-Si-nc suspensions

Peak number	Wavenumber (cm ⁻¹)	Group	Vibrational modes	Reference
1	900	SiH ₃	Degenerate deformation	[46,47,49]
2	1,113, 1,080, 1,092	Si-O-Si in SiO ₂	Stretching	[46-49]
3	880	O ₃ SiH in SiO ₂	Bending	[47,49]
4	1,200 to 1,236	Si-CH ₃ or Si-CH ₂	Symmetric bending	[50]
5	1,360	C-H	Bending	[50]
6	1,390 to 1,460	C-CH ₃ or SiCH ₃ or 2	Deformation or scissoring	[50]
7	1,710	Carboxyl		[48]
8	2,350	CO ₂	Room ambience	[47]
9	1,020	Si-OR	Stretching	[50]
10	2,880	C-CH ₂ or 3	Stretching	[50,51]
11	2,974	C-CH ₃ or Si-CH ₃	Asymmetric stretching	[50]
12	2,820	C-CH ₂	Symmetric stretching	[50]
13	1,740	Ambient water vapor		[47]

Peak positions of FTIR vibrational modes and their assignment.

spectra of the suspensions and their vibration mode assignments are listed in Table 2.

For the nanostructures with C-Si-ncs treated with acetone as solvents, different bands extending from approximately 900 to 1,260 cm⁻¹ are present. These bands (1, 2, and 9) do not have high absorbance, only the peak 4 which correspond to Si-H₃, Si-CH_n, SiOR, and Si-O-Si, respectively. There is a very small peak around 800 cm⁻¹ which is assigned to an O₃SiH bond in SiO_x. A very weak peak seems to appear at about 2,110 cm⁻¹, but it is difficult to distinguish unless compared with the other sample spectra.

For the nanostructures with C-Si-nc treated with methanol and ethanol as solvents, different bands extending from approximately 900 to 1,260 cm⁻¹ are present, with a distinct peak at 1,080 cm⁻¹ (there is also an appearance of a shoulder at approximately 1,195 cm⁻¹). HF etched Si-ncs in PSi; therefore, the spread of the band with a peak at approximately 1,080 cm⁻¹ is the same as that of C-Si-ncs with acetone as solvent; similarly, another broad band with a peak at about 880 cm⁻¹ is identified.

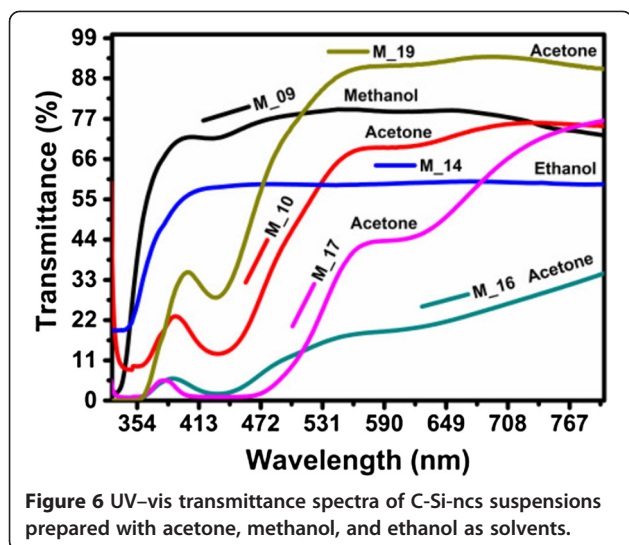
The FTIR spectra clearly show the presence of oxygen in all the samples. The broad band at around 1,080 cm⁻¹ is assigned to the Si-O-Si bond stretching. Pai et al. [52] and Lucovsky et al. [53] have shown that the position of the principal absorption band, i.e., the Si-O-Si stretching band of the Si oxide, is sensitive to the O-to-Si ratio.

According to these authors, the peak of the Si-O-Si stretching band at 1,080 cm⁻¹ corresponds to non-stoichiometric SiO_x. Therefore, it can be concluded that SiO_x is present in all samples.

This reduced sharpness of the distinction between the peak and the shoulder supports the non-stoichiometry of the Si-O-Si stretching band [53]. The origin of hydrogen in the PSi-etched Si-ncs in the form of Si-H bonds is in all possibility from the trapped moisture since the enormous surface area adsorbs moisture when exposed to the ambient atmosphere. Thus, the presence of hydrogen species can tentatively be assigned to originate from the adsorbed PSi on the surface which formed hydrogen bonds during the etching process. The samples are dominated by oxygen, too. This observation implies that the etching process replaces oxygen with hydrogen, and the hydrogen passivation is greater for HF. Although the presence of the Si-O-Si bands are also clearly detected in the C-Si-nc suspensions, it is difficult to conclude that these are residual oxides due to the exposure of the Si-ncs to the ambient atmosphere. Pi et al. [54] observed that Si-ncs get passivated exclusively by hydrogen immediately after HF etching, but signatures of Si-O-Si grow with time as the Si-ncs are exposed to the atmosphere. This is because hydrogen does not completely passivate defects such as dangling bonds at the surface of the C-Si-ncs. Then, there is a subsequent passivation by oxygen. The increase in intensity of the Si-O-Si bonding peaks at approximately 800, 1,080, and 1,113 cm⁻¹ on the oxidized Si-ncs is probably due to oxygen capture from the atmosphere by the enhanced defect centers. Therefore, the FTIR results suggest that all C-Si-nc suspensions are capable of creating isolated Si-ncs and passivating Si with hydrogen, but at the same time, creates an increase of defects at the surface. The defects at the surface increase, which are subsequently passivated with oxygen on exposure to ambient atmosphere.

UV-vis spectroscopy

The optical bandgap of the C-Si-ncs suspensions is obtained from UV-vis spectra measurements. Transmittance spectra for C-Si-nc suspensions are shown in Figure 6. The transmittance spectra of the C-Si-nc solutions with acetone as solvent are relatively high (90%) from 550 to 800 nm, as shown in Figure 6. The transmittance spectra of the C-Si-nc suspensions with methanol and ethanol are smaller than the ones obtained for samples with acetone as solvent. The Si-nc size with the different organic solvents produces a clear change in the form of the spectra and a shift towards lower wavelengths. Also, in these transmittance spectra, it is possible to observe that some curves have two or three oscillations from 300 to 600 nm; therefore, two possible regions of strong-medium absorption are present. These



absorptions can be contributions of different band-to-band transitions for extended states or localized states, as will be discussed later.

To obtain the bandgap of our solutions, we use the method of inflection point. This method is based on the minimum photon energy needed to promote electron-hole pairs. This point given to a certain wavelength indicates whether the absorption of photons is sufficient to generate electron transitions from the valence band to the conduction band; if not, these photons have a lower band-gap of the material energy. Mathematically, the inflection point is located when the second derivative is zero or does not exist. In our case, with the first derivative, it showed maximum peaks and when applied to the second derivative, these peaks are zero. But with the first derivative, it is easier; see details and the obtained band-gap energy reported in [47]. Now, the M-09 sample represents a peak at 349 nm that corresponds to an optical energy bandgap of 3.55 eV. For the M-14 sample, the point of inflection is located at 357 nm, and it corresponds to optical energy bandgap of 3.47 eV. Now, for the M-10, M-16, M-17, and M-19 samples, the derivative presents two or three peaks at different energies. For example, in M-10 and M-16, the first peaks are located at 371 and 369 nm, respectively; the second peaks are at 475 and 469 nm, in energy terms correspond to 3.34 and 3.36 eV, and 2.61 and 2.64 eV, respectively. The M-17 and M-19 samples have the first peaks at 350 and 380 nm, the second peaks at 450 and 580 nm, and the third peaks at 600 and 775 nm, which correspond to 3.54 and 3.26 eV, 2.75 and 2.13 eV, and 2.06 and 1.6 eV, respectively.

The different peaks of the derivative of transmittance spectra that have been found have been attributed to smaller particles in the colloidal solutions as in the silver colloidal solutions [55]. Other authors have reported the

same effect, but they do not say anything about these effects [50,56]. Also, the behavior of the transmittance spectra of the colloidal solutions with different solvents change depending of the solvent used [57]; in this reference, they used other method of synthesis, and the bandgap obtained in this case is in the range from 2.4 to 3.2 eV [57]. These results are similar to the ones obtained in this work, approximately 2.3 to 3.3 eV. On the other hand, according to the results here obtained, and in the case of the C-Si-nc suspensions, the electron density of states is likely to decrease with decreasing size of the Si-ncs. Then, a decrease of the absorption coefficient of Si-ncs can be understood [58]. Probably, the position of the derivative peaks can be related to the average size and distribution of Si-nc, where the position and size of the Si-ncs are dispersed, resulting in a change of the density of states due to bonds that correspond to Si-H_n, Si-O, Si-CH_n, and Si-OR.

In Figure 7, it appears that the derivative peak is dependent on the solvent, average size, and distribution of Si-nc in the range from 1.8 to 3.5 eV, where it is clear that the absorption is due to indirect transitions side to side because the first direct band (3.2 eV) is outside this range. In this case, due to the different derivative peaks, we can obtain the different optical bandgaps in only one sample and then there are different mechanical transitions. Kovalev et al. [59] found that PSi absorption is of exponential behavior in the range from 1.5 to 3.0 eV. Therefore, we considered similar C-Si-nc suspensions and propose that this is due to the absorption in the surface states and also to phonon-assisted optical absorption as expected from the indirect nature of c-Si but also direct transitions because Si-ncs are expected. In our case, we can attribute the transmittance derivative peaks' nature of the structure to the indirect and direct absorption bands because there is a fundamental connection between absorption and indirect and direct band structures of the Si-ncs and defect.

From the results of photoluminescence, the PL spectrum extends below the absorption edge of the Si-ncs (3.2 eV). Therefore, the existence of forms and Stokes photons above the bandgap indicates that the radiative recombination takes place not only between shallow trapped electron and hole states [39] but also between quantized states of electrons and holes. Some of the electrons within the nanocrystals absorb photons and relax to localized states by phonon emission or emission photon and then there recombined with holes radiatively, while some of the electrons absorb photons and directly recombine radiatively without any phonon emission to the nanocrystals. Furthermore, theoretical calculations show that the size of the nanocrystals reduces the possibility of transitions involving phonon, increasing due to the quantum size effect, where Si-ncs are

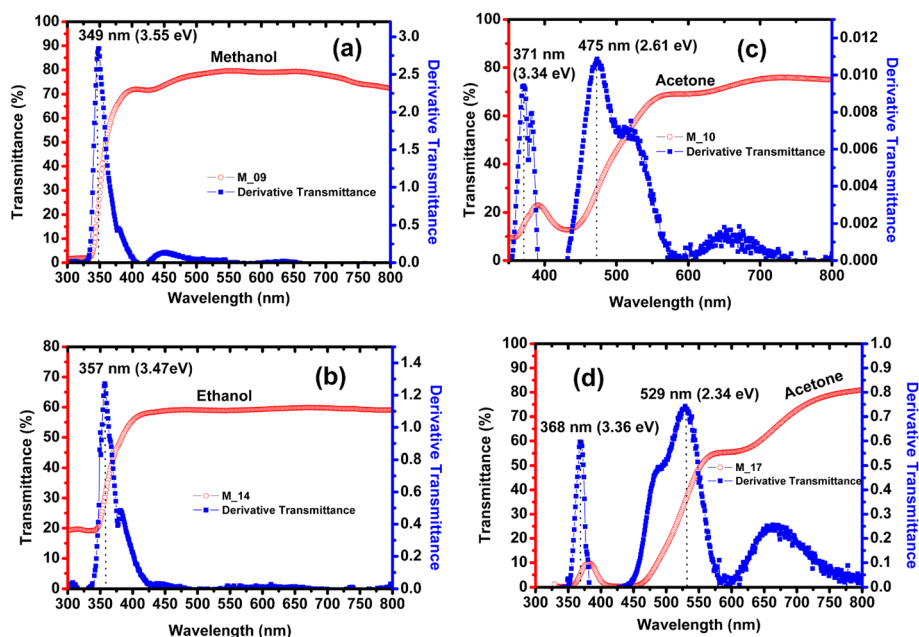


Figure 7 UV-vis transmittance spectra of C-Si-nc suspensions and derivative of transmittance spectra to obtain optical bandgap. (a) Colloidal suspension with methanol as solvent. (b) Colloidal suspension with solvent ethanol as solvent. (c and d) Colloidal suspension with acetone as solvent.

direct band structures. Therefore, the Si-ncs and defects (as shallow traps, surface states, and localized states) always take part in the process of luminescence or absorption in the Si-ncs-defects system.

X-ray diffraction

The XRD patterns of the Si-nc powders through P*Si* were obtained and presented in Figure 8. We suppose that the changes in the peak intensities and peak position indicate

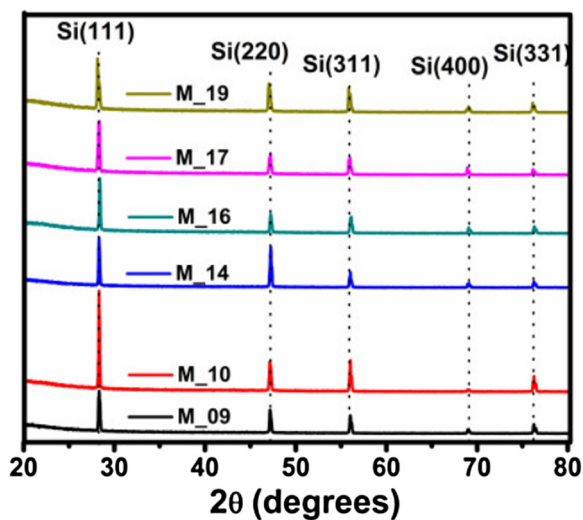


Figure 8 XRD spectra of the Si-nc powder obtained from P*Si* synthesized with different current densities.

that the concentration and size of the Si-ncs depend on the current density used to obtain the P*Si* layers.

All peaks present in the diffractograms are located close to peaks in [60] and also close to crystal planes in [47,60,61]. This indicates that Si-ncs exist in our powders. XRD data prove that these films consist of Si-ncs with preferential (111) orientation. The small additional peaks around $2\theta = 47.193^\circ$ (220), 56.023° (311), 68.989° (400), and 76.261° (331) can be connected with some metastable Si states. Using the full width at half maximum (FWHM) of the peaks around 28.346° (111), 47.193° (220), 56.023° (311), 68.989° (400), and 76.261° (331), it was possible to calculate the average size of the Si-ncs by using the Scherrer equation [62,63]. Table 3 shows a comparison between the diffraction peaks of the JCPDS card 27-1402 and those of [60], with respect to the peaks obtained from Si-nc powders in this work. The intensity of the XRD signals, which is proportional to the volume of the Si-ncs, changes with the increase of current density for five types of Si-ncs.

With the XRD spectra of Figure 9, it was found that our colloidal solutions have nanocrystals with average sizes of approximately of 6 nm and corroborated with the TEM image in the next section.

TEM images

With XRD, we find that the silicon nanocrystals with an average size of approximately 6 nm have similar sizes with those obtained with TEM images (4.34 nm). These

Table 3 Typical XRD diffraction peaks of the Si-nc powders obtained by PSi with different current densities

Ref. [47,60] peak position (PP)	Sample M-09		Sample M-10		Sample M-14		Sample M-16		Sample M-17		Sample M-19	
	PP	Size (nm)	PP	Size (nm)	PP	Size (nm)	PP	Size (nm)	PP	Size (nm)	PP	Size (nm)
28.44	28.34	41.57	28.33	98.63	28.33	61.83	28.41	72.43	28.32	43.30	28.18	52.22
47.30	47.19	44.75	47.19	42.53	47.24	60.37	47.25	41.64	47.24	39.34	47.06	32.20
56.12	56.02	50.28	56.02	122.7	56.02	56.10	56.08	38.19	55.99	37.48	55.85	56.9
69.13	68.98	48.35	68.97	39.10	68.12	32.75	69.06	80.54	68.91	60.07	69.06	99.88
76.38	76.26	44.5	76.26	40.27	76.27	39.26	76.31	38.16	76.17	44.05	76.13	48.98

The different planes of Si are indexed according to JCPDS card 27-1402.

results are similar to those reported by Ray et al. [47]. The size in the colloidal solutions based in XRD and TEM is between 4 to 6 nm. This shows that we have different sizes in our samples and our systems are polydispersed (Figure 10).

Finally, other similar works with all these characterizations have been reported by Ray et al. [47]. Their synthesis by controlled oxidation of mechanically milled silicon is an extremely slow process (100 h). The characterization realized in this work is very similar to ours. For example, in XRD, they get three peaks and nanocrystals between 14 to 30 nm in samples of powders. Similar size is obtained in our powders. TEM images show sizes of nanocrystals between 2 to 6 nm, and in our results, the size of C-Si-ncs is between 4 and 6 nm. On the other hand, with respect to FTIR, several groups with silicon oxide, silicon-hydrogen, and carbon-hydrogen bonds were obtained. Their PL spectra have some resemblance with ours because they also had double peaks of photoluminescence in the red region. Similar behavior is obtained in the UV-vis spectra. The bandgap was calculated using the same method, with energies of the same order as our results. This demonstrates that there is a method simpler to get results like that of Ray et al. [47]. Regarding the working life of the

colloidal solutions, our samples were synthesized more than 6 months ago and are still presenting the same intense photoluminescence. Even when the solvent evaporates, depositing the same solvent would result to the same PL. These materials have a lot of application because they exhibit unique physical and electronic properties which can be used as substitutes of SRO films, such as thin film to devices, where the C-Si-ncs can be used to different applications such as photovoltaic, photodetectors, and emission light.

Conclusions

In summary, in this study, the process was performed to remove the luminescent PSi nanostructures by scraping the PSi from electrochemically etched silicon wafer. The obtained powders were milled together with a selected solvent, and colloidal suspensions with silicon nanocrystals (C-Si-ncs) were obtained. On the other hand, HF etching is capable of producing free-standing isolated spherical quantum dots of Si with nanometric dimensions. The FTIR study revealed that along with the

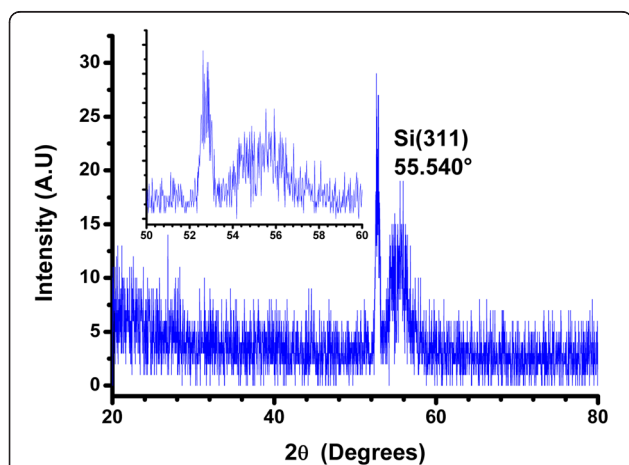


Figure 9 XRD spectra of the C-Si-ncs with acetone. Inset shows an approximation of the peak Si (311).

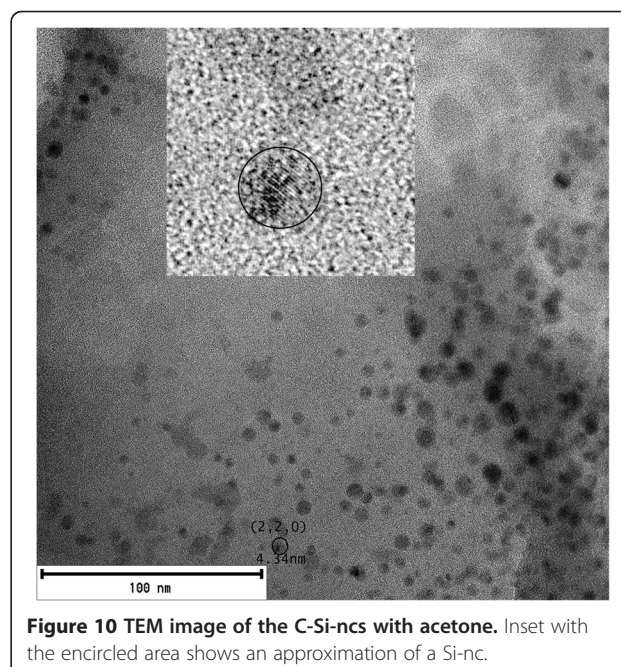


Figure 10 TEM image of the C-Si-ncs with acetone. Inset with the encircled area shows an approximation of a Si-nc.

creation of isolated Si-ncs and hydrogen passivated Si, an increment of defects is also introduced at the surface of the Si-ncs; these defects are subsequently passivated by oxygen on exposure to ambient atmosphere. The PL characteristics of the C-Si-nc suspensions of these nanostructures are characterized by double peaks, and the observations provide direct evidence for quantum confinement-induced widened bandgap transitions and oxide-related interface state-mediated transitions and also allow us to experimentally distinguish between the contributions of the two transition mechanisms. Therefore, the PL emission can be correlated with quantum effects and defects in C-Si-nc suspensions, where also the absorption FTIR spectra show peaks associated with Si compounds. Those are also associated with defects. Then, a relationship between the composition and PL was obtained. Also, the different Si-nc sizes and organic solvents of the C-Si-nc suspensions produce a clear change of the transmittance spectra and a shift towards lower wavelengths.

Competing interests

The authors declare that they have no competing interests.

Authors' contributions

JALL and AGR participated in the growth of the films; carried out the FTIR, photoluminescence, and UV-vis measurements; and drafted the manuscript. JFFG and JCL conducted the photoluminescence measurements. EGB and JMJ conducted the XRD measurements. AGR coordinated the study. JALL provided the idea and supervised the study. All authors read and approved the final manuscript.

Authors' information

JALL is currently a researcher and professor in the Science Institute-Center of Investigation for Semiconductors Devices (IC-CIDS) from Autonomous University of Puebla, Mexico. He has been working on structural, electrical, and optical characterization of materials and MOS structures. His research interest is the physics and technology of material nanostructures and silicon devices. Additionally, his research interests are nanotechnology, material characterization, and optoelectronic devices such as sensor, LEDs, and solar cells. EGB is a researcher and instructor in the Research Center of Semiconductor Devices of the Institute of Science, Benemérita Universidad Autónoma de Puebla, México. She has been working mainly on the synthesis of semiconductor materials and their optic, morphologic, and photocatalytic properties, and their composition. Her actual research interest is on the synthesis, characterization, and applications of porous silicon.

Acknowledgements

This work has been partially supported by CONACYT-154725, PIFI-2014, PROMEP, and VIEP-BUAP-2014. The authors acknowledge IFUAP, INAOE, and Department of Physics and Astronomy (UTSA) Laboratories for their help in the sample measurements.

Received: 13 May 2014 Accepted: 2 October 2014

Published: 13 October 2014

References

1. Liu C-Y, Holman ZC, Kortshagen UR: Hybrid solar cells from P3HT and silicon nanocrystals. *Nano Lett* 2009, **9**(Suppl 1):449-452.
2. Kim B-H, Cho C-H, Mun J-S, Kwon M-K, Park T-Y, Kim JS, Byeon CC, Lee J, Park S-J: Enhancement of the external quantum efficiency of a silicon quantum dot light-emitting diode by localized surface plasmons. *Adv Mater* 2008, **20**(Suppl 16):3100-3104.
3. Kumar V: Metal encapsulated clusters of silicon: silicon fullerenes and other polyhedral forms. In *Nanosilicon*. Edited by Kumar V. London: Elsevier; 2007:217-255.
4. Lannoo M, Delerue C, Allan G: Theory of radiative and nonradiative transitions for semiconductor nanocrystals. *J Lumin* 1996, **70**(Suppl 1):170-184.
5. Smith A, Yamani ZH, Roberts N, Turner J, Habbal SR, Granick S, Nayfeh MH: Observation of strong direct-like oscillator strength in the photoluminescence of si nanoparticles. *Phys Rev B* 2005, **72**(Suppl 20):205307.
6. Canham LT: Silicon quantum wire array fabrication by electrochemical and chemical dissolution of wafers. *Appl Phys* 1990, **57**(Suppl 10):1046-1048.
7. Martínez OC: Síntesis y caracterización de óxido rico en silicio a bajas temperaturas. In *Masters thesis*. Instituto Nacional de Astrofísica Óptica y Electrónica (INAOE); 2011.
8. Pileni MP: Control of size and shape of inorganic nanocrystals at various scales from nano to macrodomains. *J Phys Chem C* 2007, **111**(Suppl 26):9019-9038.
9. Hartlen DK, Athanasopoulos APT, Kitaev V: Facile preparation of highly monodisperse small silica spheres (15 to >200 nm) suitable for colloidal templating and formation of ordered arrays. *Langmuir* 2008, **24**(Suppl 5):1714-1720.
10. Jiang P, Bertone JF, Colvin VL: A lost-wax approach to monodisperse colloids and their crystals. *Science* 2001, **291**(Suppl 5503):453-457.
11. Narayanan R, El-Sayed MA: Shape-dependent catalytic activity of platinum nanoparticles in colloidal solution. *Nano Lett* 2004, **4**(Suppl 7):1343-1348.
12. Bell TA: The impact of nanoscience on heterogeneous catalysis. *Science* 2003, **299**(Suppl 5613):1688-1691.
13. Zhang J, Liu J, Peng Q, Wang X, Li Y: Nearly monodisperse Cu₂O and CuO nanospheres: preparation and applications for sensitive gas sensors. *Chem Mater* 2006, **18**(Suppl 4):867-871.
14. Kim J, Grate JW: Single-enzyme nanoparticles armored by a nanometer-scale organic/inorganic network. *Nano Lett* 2003, **3**(Suppl 9):1219-1222.
15. Deng H, Li X, Peng Q, Wang X, Chen J, Li Y: Monodisperse magnetic single-crystal ferrite microspheres. *Angew Chem Int Ed* 2005, **44**(Suppl 18):2782-2785.
16. Xia Y, Gates B, Yin Y, Lu Y: Monodispersed colloidal spheres old materials with new applications. *Adv Mater* 2000, **12**(Suppl 10):693-713.
17. Matijevic E: Uniform inorganic colloid dispersions. Achievements and challenges. *Langmuir* 1994, **10**(Suppl 1):8-16.
18. Negen WW, Shook I: Equilibrium properties of suspensions. *Adv Colloid Interf Sci* 1984, **21**(Suppl 1):119-194.
19. Matijevic E: Preparation and properties of uniform size colloids. *Chem Mater* 1993, **5**(Suppl 4):412-426.
20. Brinker CJ, Scherer GW: *Sol-gel Science: The Physics and Chemistry of Sol-gel Processing*. New York: Academic; 1989.
21. Zhou Z, Brus L, Friesner R: Electronic structure and luminescence of 1.1- and 1.4-nm silicon nanocrystals: oxide shell versus hydrogen passivation. *Nano Lett* 2003, **3**:163-167.
22. Fojtik A, Henglein A: Luminescent colloidal silicon particles. *Chem Phys Lett* 1994, **221**:363-367.
23. Chen XY, Lu YF, Wu YH, Cho BJ, Liu MH, Dai DY, Song WD: Mechanisms of photoluminescence from silicon nanocrystals formed by pulsed-laser deposition in argon and oxygen ambient. *J Appl Phys* 2003, **93**:6311.
24. Vanhellefont J, De Gryse O, Clauws P: Critical precipitate size revisited and implications for oxygen precipitation in silicon. *J Appl Phys* 2005, **86**:221903.
25. Shimizu-Iwayama T, Fujita K, Nakao S, Saitoh K, Fujita T, Itoh N: Visible photoluminescence in Si⁺-implanted silica glass. *J Appl Phys* 1994, **75**:7779-7783.
26. Min KS, Shcheglov KV, Yang CM, Atwater HA, Brongersma M L, Polman A: Defect-related versus excitonic visible light emission from ion beam synthesized Si nanocrystals in SiO₂. *Appl Phys Lett* 1996, **69**:2033-2035.
27. Littau KA, Szajowski PJ, Muller AJ, Kortan AR, Brus LE: A luminescent silicon nanocrystal colloid via a high-temperature aerosol reaction. *J Phys Chem* 1993, **97**:1224-1230.
28. Holunga DM, Flagan RC, Atwater HA: A scalable turbulent mixing aerosol reactor for oxide-coated silicon nanoparticles. *Indust Eng Chem Res* 2005, **44**:6332-6341.
29. Zhang Q, Bayliss SC, Hutt DA: Blue photoluminescence and local structure of Si nanostructures embedded in SiO₂ matrices. *Appl Phys Lett* 1995, **66**:1977-1979.

30. Schmidt JU, Schmidt B: Investigation of Si nanocluster formation in sputter-deposited silicon sub-oxides for nanocluster memory structures. *Mater Sci Eng B* 2003, **101**:28–33.
31. Lin CF, TsengW T, Feng MSJ: Formation and characteristics of silicon nanocrystals in plasma-enhanced chemical vapor-deposition silicon-rich oxide. *Appl Phys* 2000, **87**:2808–2815.
32. Nozaki T, Sasaki K, Ogino T, Asahi D, Okazaki K: Microplasma synthesis of tunable photoluminescent silicon nanocrystals. *Nanotechnology* 2007, **18**:235603.
33. Saunders WA, Sercel PC, Lee RB, Atwater H, Vahala KJ, Flanagan RC, Escorsi-Aparcio EJ: Synthesis of luminescent silicon clusters by spark ablation. *Appl Phys Lett* 1993, **63**:1549–1551.
34. Kahler U, Hofmeister H: Visible light emission from Si nanocrystalline composites via reactive evaporation of SiO. *Opt Mater* 2001, **17**:83–86.
35. Valenta J, Jenada P, Dohnalová K, Niznansky D, Vácha F, Linnros J: Colloidal suspensions of silicon nanocrystals: from single nanocrystals to photonic structures. *Opt Mater* 2005, **27**(Suppl 5):1046–1049.
36. Nobuaki N, Ik S: Luminescent porous silicon synthesized by visible light irradiation. *Appl Phys Lett* 1993, **62**:1429.
37. Nayfeh MH, Rao S, Nayfeh OM, Smith A, Therrien J: UV photodetectors with thin-film Si nanoparticles active medium. *IEEE Trans Nanotechnol* 2005, **4**(Suppl 6):660–668.
38. Tilley RD, Warner JH, Yamamoto K, Matsui I, Fujimori H: Micro-emulsion synthesis of monodisperse surface stabilized silicon nanocrystals. *Chem Commun* 2005, **14**:1833–1835.
39. Lehman V, Gösele U: Porous silicon formation: a quantum wire effect. *Appl Phys Lett* 1991, **58**:856.
40. Proot JP, Delerue C, Allan G: Electronic structure and optical properties of silicon crystallites: application to porous silicon. *Appl Phys Lett* 1992, **61**(Suppl 16):1948.
41. Koch F, Petrova-Koch V, Muschik T: The luminescence of porous Si: the case for the surface state mechanism. *J Lumin* 1993, **57**(Suppl 1):271–281.
42. Prokes SM: Light emission in thermally oxidized porous silicon: evidence for oxide-related luminescence. *Appl Phys Lett* 1993, **62**(Suppl 25):3244–3246.
43. Brandt MS, Fuchs HD, Stutzmann M, Weber J, Cardona M: The origin of visible luminescence from porous silicon: a new interpretation. *Solid State Commun* 1992, **81**(Suppl 4):307.
44. Fauchet PM: Photoluminescence and electroluminescence from porous silicon. *J Lumin* 1996, **70**(Suppl 1):294–309.
45. Wolkin MV, Jorne J, Fauchet PM, Allan G, Delerue C: Electronic states and luminescence in porous silicon quantum dots: the role of oxygen. *Phys Rev Lett* 1999, **82**(Suppl 1):197.
46. Vásquez-A MA, Rodríguez GÁ, García-Salgado G, Romero-Paredes G, Peña-Sierra R: FTIR and photoluminescence studies of porous silicon layers oxidized in controlled water vapor conditions. *Rev Mex Fis* 2007, **53**(Suppl 2):431–435.
47. Ray M, Hossain SM, Klie RF, Banerjee K, Ghosh S: Free standing luminescent silicon quantum dots: evidence of quantum confinement and defect related transitions. *Nanotechnology* 2010, **21**(Suppl 50):9.
48. Venkatathri N: Preparation of silica nanoparticle through coating with octyldecylmethoxy silane. *Indian J Chem* 2007, **46A**(Suppl 12):1955–1958.
49. Xie YH, Wilson WL, Ross FM, Mucha JA, Fitzgerald EA, Macaulay JM, Harris TD: Luminescence and structural study of porous silicon films. *J Appl Phys* 1992, **71**(Suppl 5):2403–2407.
50. Yang CS, Bley RA, Kauzlarich SM, Lee HWH, Delgado GR: Synthesis of alkyl-terminated silicon nanoclusters by a solution route. *J Am Chem Soc* 1999, **121**(Suppl 22):5191–5195.
51. Lee S, Chin CS, Cho WJ, Han IK, Park YJ, Choi WJ, Song JD, Lee JI: Optical properties of silicon nanoparticles by ultrasound-induced solution method. *Jpn J Appl Phys* 2004, **43**(Suppl L):784-L 786.
52. Pai PG, Chao SS, Takagi Y, Lucovsky G: Infrared spectroscopic study of SiO_x films produced by plasma enhanced chemical vapor deposition. *J Vacuum Sci Tech A* 1986, **4**(Suppl 3):689.
53. Lucovsky G, Yang J, Chao SS, Tyler JE, Czubatjy W: Oxygen-bonding environments in glow discharge-deposited amorphous silicon-hydrogen alloy films. *Phys Rev B* 1983, **28**(Suppl 6):3225.
54. Pi XD, Mangolini L, Campbell SA, Kortshagen U: Room-temperature atmospheric oxidation of Si nanocrystals after HF etching. *Phys Rev B* 2007, **75**(Suppl 8):085423.
55. Brause R, Möltgen H, Kleinermanns K: Characterization of laser-ablated and chemically reduced silver colloids in aqueous solution by UV/VIS spectroscopy and STM/SEM microscopy. *Applied Physics B* 2002, **75**(Suppl 6):711–716.
56. Morris CA, Anderson ML, Stroud RM, Merzbacher CI, Rolison DR: Silica sol as a nanogluue: flexible synthesis of composite aerogels. *Science* 1999, **284**(5414):622–624.
57. Umezu I, Minami H, Senoo H, Sugimura A: Synthesis of photoluminescent colloidal silicon nanoparticles by pulsed laser ablation in liquids. *J Phys* 2007, **59**(Suppl 1):392.
58. Zhixun M, Xianbo L, Gonglin K, Junhao C: Absorption spectra of nanocrystalline silicon embedded in SiO₂ matrix. *Appl Phys Lett* 1999, **75**(Suppl 13):1857.
59. Kovalev D, Polisski G, Ben-Chorin M, Diener J, Koch F: The temperature dependence of the absorption coefficient of porous silicon. *J Appl Phys* 1996, **80**(Suppl 10):5978.
60. U.S. Department of Commerce, National Bureau of Standards (US): *Monographs 25*. Washington, D.C; 1976. catalog C13.44:25/sec 12.
61. Han PG, Poon MC, Sin KO, Wong M: Photoluminescent porous polycrystalline silicon. In *Electron Devices Meeting, 1995, Proceedings 1995 IEEE Hong Kong*. 2–5.
62. Keijser TH, Langford JJ, Mittemeijer EJ, Vogels ABP: Use of the Voigt function in a single-line method for the analysis of X-ray diffraction line broadening. *J Appl Crystallography* 1982, **15**:308–314.
63. Guinier A: *X-ray Diffraction in Crystals, Imperfect Crystals, and Amorphous Bodies*. San Francisco: W. H. Freeman and Co; 1963.

doi:10.1186/1556-276X-9-571

Cite this article as: Luna López et al.: Synthesis of colloidal solutions with silicon nanocrystals from porous silicon. *Nanoscale Research Letters* 2014 9:571.

Submit your manuscript to a SpringerOpen® journal and benefit from:

- Convenient online submission
- Rigorous peer review
- Immediate publication on acceptance
- Open access: articles freely available online
- High visibility within the field
- Retaining the copyright to your article

Submit your next manuscript at ► springeropen.com